

Etienne Labyt  
Tilman Sander  
Ronald Wakai *Editors*

# Flexible High Performance Magnetic Field Sensors

On-Scalp Magnetoencephalography  
and Other Applications



Springer


# Flexible High Performance Magnetic Field Sensors

Etienne Labyt • Tilmann Sander • Ronald Wakai  
Editors

# Flexible High Performance Magnetic Field Sensors

On-Scalp Magnetoencephalography and  
Other Applications

### *Editors*

Etienne Labyt   
Mag4Health  
Grenoble, France

Ronald Wakai  
Medical Physics  
University of Wisconsin  
Madison, WI, USA

Tilmann Sander   
Biosignals (Magnetoencephalography)  
Physikalisch-Technische Bundesanstalt  
Berlin, Germany

ISBN 978-3-031-05362-7

ISBN 978-3-031-05363-4 (eBook)

<https://doi.org/10.1007/978-3-031-05363-4>

© The Editor(s) (if applicable) and The Author(s), under exclusive license to Springer Nature Switzerland AG 2022

This work is subject to copyright. All rights are solely and exclusively licensed by the Publisher, whether the whole or part of the material is concerned, specifically the rights of translation, reprinting, reuse of illustrations, recitation, broadcasting, reproduction on microfilms or in any other physical way, and transmission or information storage and retrieval, electronic adaptation, computer software, or by similar or dissimilar methodology now known or hereafter developed.

The use of general descriptive names, registered names, trademarks, service marks, etc. in this publication does not imply, even in the absence of a specific statement, that such names are exempt from the relevant protective laws and regulations and therefore free for general use.

The publisher, the authors, and the editors are safe to assume that the advice and information in this book are believed to be true and accurate at the date of publication. Neither the publisher nor the authors or the editors give a warranty, expressed or implied, with respect to the material contained herein or for any errors or omissions that may have been made. The publisher remains neutral with regard to jurisdictional claims in published maps and institutional affiliations.

This Springer imprint is published by the registered company Springer Nature Switzerland AG  
The registered company address is: Gewerbestrasse 11, 6330 Cham, Switzerland

# Preface

Magnetoencephalography (MEG) is an established method for neuroscience research and clinical applications, most notably in epilepsy surgery planning. As practiced over the last 35 years, however, MEG suffers from significant limitations imposed by the use of helium cooled, low-critical temperature superconducting quantum interference devices (low-Tc SQUIDs), on which commercial systems are presently based.

New sensors, such as nitrogen cooled high-Tc SQUIDs and optically pumped magnetometers (OPMs), remove several of the major limitations of existing systems as they can be placed anywhere on the scalp and in positions adapted to an individual's head size and shape, and as required by the neuroimaging question at hand. The nearly simultaneous and pioneering recordings of neural activity with OPMs and high-Tc SQUIDs over 10 years ago spawned the rapidly growing field of on-scalp, "conformal" MEG. Since then, theory and experiment have been used to demonstrate the advantages of on-scalp MEG for improving neuromagnetic signal levels and imaging resolution, as compared to low-Tc SQUID MEG systems. Several MEG studies have also been reported with innovative experimental paradigms, only feasible with on-scalp MEG. Concomitant with this innovation in MEG are OPM applications in general biomagnetism, such as for magnetocardiography and magnetic nanoparticles, and advances in other sensor technologies such as magneto resistive (MR) magnetometers.

This volume is motivated by the need for an overview of the recent proliferation of biomagnetism applications based on new sensor technologies. While some physics background is provided, a distinguishing feature of this work is the focus on application-driven system integration issues. Several approaches to conformal MEG are presently being developed: both OPMs and high-Tc SQUIDs can be configured in single- or multi-channel systems that, in the end, move the field closer to the whole-head coverage and beyond present commercial low-Tc SQUID systems. The latest advances in this domain will be presented, such as multi-channel sensors based on single gas cells, various atomic species in sensors, and free induction decay readout. Together with the hardware, the methods of signal condition and parameter extraction will be covered not as single chapters, but each approach is a

combination of sensing unit and processing pipeline. On-scalp MEG systems allow for a complete redesign of magnetic shielding due to their reduced size compared to current commercial systems. Innovative solutions of magnetic shielding suitable for on-scalp MEG recordings are described.

Industry-based physicists and engineers contributed to this work; however, all authors write here in their capacity as scientists. An author's affiliation with a commercial entity should not be viewed as an endorsement, but rather a desire to inform readers of the critical technical innovation taking place at companies.

Following the introduction, the book contains three major sections: OPM System Development; MEG Applications; and MCG, MRX, and Other Applications. Clearly the focus is on OPMs, but other technologies have their distinctive merits and are included in the appropriate sections. The chapters vary in length, and modest overlap is permitted to make them reasonably self-contained.

The editors thank all the contributors for taking the time to write their chapters and for their patience until the work was complete. Assistance from students and colleagues in reviewing is gratefully acknowledged. We hope that this book will be valuable to researchers and students alike. Topics in this rapidly developing field omitted from this volume will find space in the next edition.

Grenoble, France  
Berlin, Germany  
Madison, WI, USA

Etienne Labyt  
Tilmann Sander  
Ronald Wakai

# Contents

## Part I OPM and System Developments

<b>1</b>	<b>Optically Pumped Magnetometers for Biomagnetic Measurements ..</b>	<b>3</b>
	Michael V. Romalis	
<b>2</b>	<b>Optically Pumped Magnetometers Compatible with Large Transient Magnetic Fields .....</b>	<b>17</b>
	Nicholas Nardelli, Sean Krzyzewski, and Svenja Knappe	
<b>3</b>	<b>Small Animal Biomagnetism Applications.....</b>	<b>33</b>
	Kasper Jensen, Bo Hjorth Bentzen, and Eugene S. Polzik	
<b>4</b>	<b>Supine OPM-MEG in Multilayer Cylindrical Shield .....</b>	<b>49</b>
	Jingwei Sheng, Dongxu Li, Shuangai Wan, Jie Qin, and Jia-Hong Gao	
<b>5</b>	<b>Ambulatory MEG Arrays .....</b>	<b>63</b>
	V. Shah, J. Osborne, and C. Doyle	

## Part II MEG Applications

<b>6</b>	<b>Tri-axial Helium-4 Optically Pumped Magnetometers for MEG .....</b>	<b>79</b>
	A. Palacios-Laloy, M. Le Prado, and E. Labyt	
<b>7</b>	<b>Person-Sized Magnetoencephalography Systems with Optically Pumped Magnetometers .....</b>	<b>111</b>
	Peter D. D. Schwindt and Amir Borna	
<b>8</b>	<b>On-scalp MEG with High-<math>T_c</math> SQUIDS .....</b>	<b>143</b>
	Justin F. Schneiderman	
<b>9</b>	<b>Fiber-Coupled OPM in Purely Coil-Shielded Environment .....</b>	<b>161</b>
	Teng Wu, Xiang Peng, Jingbiao Chen, and Hong Guo	
<b>10</b>	<b>SERF-OPM Usability for MEG in Two-Layer-Shielded Rooms .....</b>	<b>179</b>
	Vojko Jazbinšek, Urban Marhl, and Tilmann Sander	

<b>11</b>	<b>Turning OPM-MEG into a Wearable Technology</b> .....	195
	Natalie Rhodes, Niall Holmes, Ryan Hill, Gareth Barnes, Richard Bowtell, Matthew Brookes, and Elena Boto	
<b>Part III MCG, MRX, and Other Applications</b>		
<b>12</b>	<b>OPM Gradiometer for Magnetorelaxometry</b> .....	227
	A. Prospero, J. R. A. Miranda, and O. Baffa	
<b>13</b>	<b>Unshielded High-Bandwidth Magnetorelaxometry of Magnetic Nanoparticles with Optically Pumped Magnetometers</b> .....	247
	Victor Lebedev, Aaron Jaufenthaler, Thomas Middelmann, and Daniel Baumgarten	
<b>14</b>	<b>Adult Magnetocardiography: Principles and Clinical Practice</b> .....	267
	Vineet Erasala, Anthony Senagore, Peeyush Shrivastava, Rhea Malhotra, Emmanuel Setegn, and Robert Sokolowski	
<b>15</b>	<b>Fetal Magnetocardiography with OPMs</b> .....	283
	Ronald Wakai	
<b>16</b>	<b>Emerging MR Sensors for Biomagnetic Measurements</b> .....	299
	Yoshiaki Adachi, Shigenori Kawabata, Tetsuro Tatsuoka, and Yasushi Terazono	
	<b>Index</b> .....	313



## About the Editors

**Dr. Etienne Labyt** is a Senior Expert Engineer in MEG/EEG imaging at the French Alternative Energies and Atomic Energy Commission. He is working on helium optically pumped magnetometers for MEG imaging. Since February 2022, he is involved in Mag4Health company as chief medical officer.

**Dr. Tilmann Sander** is a senior scientist in the working group “Optical Magnetometry” at Physikalisch-Technische Bundesanstalt. His research interest is magnetoencephalography and the associated signal conditioning by signal processing. His current focus is assessment of OPM-MEG as complement or alternative to SQUID-MEG.

**Prof. Ronald Wakai** is a Professor in the Department of Medical Physics at the University of Wisconsin. His research involves biomedical applications of magnetic sensors and signal processing. The focus of his current research is fetal magnetocardiography.

# **Part I**

## **OPM and System Developments**

# Chapter 1

## Optically Pumped Magnetometers for Biomagnetic Measurements



Michael V. Romalis

**Abstract** This review will summarize general aspects of optically pumped magnetometers and some of their features and challenges for applications to biomagnetic measurements. Such sensors rely on Larmor spin precession of optically polarized paramagnetic atoms in the magnetic field to be measured. Several optical magnetometry methods have been developed with sensitivity approaching or even exceeding that of SQUID magnetometers. Atomic sensors can be made quite compact, allowing measurements of magnetic fields closer to biomagnetic field sources. Present efforts are focused on the development of inexpensive systems with many small sensors that are robust in the presence of external magnetic field interference.

**Keywords** Atomic magnetometer · Optically pumped magnetometer · Bloch equation · Shot noise · Spin projection noise · Alkali metal magnetometer · Spin exchange relaxation free · Scalar magnetometer · Vector magnetometer

### 1.1 Introduction

This chapter will provide a basic introduction to the physics of optically pumped magnetometers with focus on their application to biomagnetic measurements. Broadly speaking, optically pumped magnetometers use light to manipulate quantum states of atoms in order to measure atoms' interactions with the magnetic field. The goal is to find a system where atoms behave as nearly isolated particles and only have well-defined interactions with the external magnetic field. The term *atomic magnetometer* will also be used, and it is often avoided in the biomagnetism literature to eliminate negative association with nuclear energy. This chapter will present a relatively colloquial description of atomic magnetometers, pointing out

---

M. V. Romalis (✉)

Physics Department, Princeton University, Princeton, NJ, USA

e-mail: [romalis@princeton.edu](mailto:romalis@princeton.edu)

general features with a minimum level of mathematical details. It does not attempt to provide a thorough review of the literature or to point out all exceptions to the most commonly used methods in optical magnetometry.

Atoms with a finite spin angular momentum but zero orbital angular momentum are typically chosen in order to maximize sensitivity to magnetic fields while reducing the effects of atomic collisions. The populations of the atomic quantum spin states can be manipulated and measured using optical atomic transitions, and this process is called optical pumping. Thus at a conceptual level, an optically pumped magnetometer can be visualized as a collection of isolated atoms interacting with a common laser beam. What makes atomic magnetometers remarkable is that a practical implementation of such device is not very different from the idealized picture. Atoms are usually held in a sealed glass container, called a cell. Random thermal motion of the atoms has no effect on their spin states, while the effects of atomic collisions can be arranged to be small. Thus, the main elements of atomic magnetometers are fairly simple and robust. Most of the effort is focused on the development of optimal methods to manipulate and measure the quantum spin states. For biomagnetic measurements, other challenges include miniaturization of the sensors, improving their performance in the presence of ambient magnetic field noise and reducing the complexity of the system.

Given relative simplicity of optically pumped magnetometers, it is not surprising that they were already developed in 1950s [1], soon after demonstration of optical pumping [2, 3]. Their initial use was mostly focused on geophysical applications [4], but already in 1960s atomic magnetometers of sufficient sensitivity have been demonstrated with a suggestion to use them for detection of biomagnetism [5]. The first detailed study of biomagnetic fields using atomic sensors was performed in 1970s [6]. They were able to detect fields from the heart, muscles, and eyes, while brain magnetic fields were seen “at the noise level of the detector.” Several more detailed studies of heart magnetic fields were subsequently performed [7]. Early atomic magnetometers used electric discharge lamps containing the same type of atoms to generate light for optical pumping and optical readout. With the development of readily available diode lasers, the interest in optical magnetometers for biomagnetic field detection was revived, and detection of heart [8] and brain [9] magnetic fields was demonstrated in 2000s. Since then, optical magnetometry has developed in a number of different directions as discussed in this volume.

## 1.2 General Features of Atomic Magnetometer Operation

Magnetic field detection using atomic spins can be conceptually broken into three steps. In the first step, optical pumping with a laser creates a non-equilibrium distribution of populations among quantum spin states. In the second step, the spin states evolve in the presence of the magnetic field, and in the final step, the quantum state of the spins is readout using a laser beam. In some magnetometer implementations, one laser is used for both optical pumping and detection, while

others have separate pump and probe lasers. Similarly, some implementations involve pulsed operation with a short optical pumping interval followed by free spin precession and detection phase. Others use continuous operation, where optical pumping, spin precession, and detection all occur at the same time. In the development of atomic magnetometers for biomagnetic applications, there is always a tension between more complicated approaches that offer better sensitivity and simpler detection schemes that are more robust.

The evolution of spins in optically pumped magnetometers can often be understood in terms of Bloch equations that describe precession of a spin-1/2 particle in a magnetic field:

$$\frac{d\mathbf{S}}{dt} = \gamma \mathbf{S} \times \mathbf{B} - \left\{ \frac{S_x}{T_2}, \frac{S_y}{T_2}, \frac{S_z}{T_1} \right\} + R(t) \left( \frac{\mathbf{s}}{2} - \mathbf{S} \right). \quad (1.1)$$

Here,  $\mathbf{S}$  denotes the average vector expectation value of the atom's spin; for an atomic ensemble, it can range in magnitude from 0 to 1/2.  $\gamma$  is the spin's gyromagnetic ratio and  $\mathbf{B}$  is the magnetic field vector. The basic solution of Bloch equations is given by precession of the spin vector around the total magnetic field vector, described by the first term in Eq. (1.1). The precession frequency, also called the Larmor frequency, is given by  $\omega_L = \gamma |\mathbf{B}|$ . The gyromagnetic ratio  $\gamma$  for atoms with an unpaired electron spin is on the order of Bohr magneton  $\mu_B$  divided by  $\hbar$ . This corresponds to a spin precession frequency on the order of 300 kHz in Earth's magnetic field but only a frequency on the order of 1 mHz due to a typical biomagnetic field. Fortunately, about  $10^{12}$  atoms can be measured simultaneously, so by averaging their spin signals, one can reduce the quantum spin state uncertainty by a factor of  $10^6$ . So one does not need to wait for 1000 sec but can in fact resolve a 1 mHz frequency shift in about 1 msec, providing sufficient bandwidth to resolve most biomagnetic signals.

The duration of coherent spin precession is governed by the spin relaxation times, given by the second term in Eq. (1.1). If the total magnetic field vector points along  $\hat{z}$  direction, then the relaxation of the transverse spin components  $S_x$  and  $S_y$  is given by the transverse relaxation time  $T_2$ , and the relaxation of the longitudinal component  $S_z$  is given by the longitudinal relaxation time  $T_1$ . This nomenclature is adapted from NMR terminology, where Bloch equations are also used to describe spin dynamics. The relaxation times in optically pumped magnetometers are typically on the order of 1 msec. There are two general approaches for making the spin relaxation time longer, which improves the sensitivity of magnetometers. One approach uses a special low-polarizability coating on cell walls that allows atoms to bounce off the walls without losing their spin orientation [10]. Another approach uses a buffer gas that slows down the diffusion of atoms to cell walls. Collisions with the buffer gas molecules then limit the spin relaxation time. One can increase the density of optically pumped atoms until the sensitivity becomes ultimately limited by collisions between the spin-polarized atoms themselves. These relaxation processes are more complicated and depend on the magnetic field and degree of spin polarization, as will be discussed later in the chapter.

A distinguishing feature of optically pumped magnetometers compared with NMR is the presence of the last term in Eq. (1.1) representing optical pumping. Here, the vector  $\mathbf{s}$  denotes the degree of circular polarization and the direction of the optical pumping light. The magnitude of  $\mathbf{s}$  can range from 0 to 1 for fully circularly polarized light, while the vector direction is parallel to the propagation direction of the light and indicates the sense of circular polarization.  $R(t)$  is the optical pumping rate that can be modulated in time in a number of ways. For example,  $R(t)$  can represent turning on and off of the pump laser for a pulsed magnetometer or it can be modulated at the Larmor precession frequency to excite the precession of the atoms as in a Bell–Bloom magnetometer [11]. The magnetic field  $\mathbf{B}$  can also have a time dependence, not only due to the signals being measured, but also from external magnetic field modulations that are used to manipulate the precession of the spins.

The sensor measurement modes can be separated into two types based on the value of the total magnetic field: zero-field and total field measurement. For zero-field sensors, the total magnetic field at the location of the spins is small, so the frequency of spin precession around the magnetic field is smaller than the transverse relaxation rate,  $\omega_L < 1/T_2$ . In this regime, one can think of the spin direction slowly evolving in response to the instantaneous magnetic field vector, optical pumping, and relaxation rates. The measured signal is sensitive to one or more vector field components. The vector axes of the magnetometer are imposed by the experimental geometry, such as direction of a laser beam or magnetic field modulation.

The second type of optically pumped magnetic field sensors, called scalar sensors or total field sensors, operates in the regime where the Larmor frequency  $\omega_L \gg 1/T_2$ , so the atoms complete many precession cycles during one coherence time. In this regime, the frequency of spin precession, which is proportional to the total magnetic field, is the main observable. Usually, a constant magnetic field  $B_0$ , called a bias field, is much larger than any biomagnetic field vector  $\mathbf{b}$ . As a result, the Larmor frequency  $\omega_L = \gamma \sqrt{b_x^2 + b_y^2 + (B_0 + b_z)^2} \approx \gamma(B_0 + b_z)$ . So a scalar magnetometer is primarily sensitive to the projection of the biomagnetic field onto the direction of the total magnetic field  $B_0$ .

Bloch equations capture many features of atomic magnetometer operation but do not provide a complete description because most atoms used for optically pumped magnetometers are not spin-1/2 systems. Alkali-metal atoms (Cs, Rb, or K) are typically used because they have an unpaired electron spin in the ground state, relatively high vapor density, and a convenient optical transition. These atoms also have a nuclear spin  $I$ , and hyperfine interactions tightly couple electron and nuclear spin states into eigenstates of the total angular momentum  $F$ ,  $\mathbf{F} = \mathbf{S} + \mathbf{I}$ . Spin evolution can then be described by a density matrix involving multiple quantum states. Some magnetometer approaches use higher polarization moments, such as alignment, where the average value of the vector  $\mathbf{F}$  is zero, but spin states have a preferential alignment along an axis [12].

Optical pumping typically uses the so-called  $D_1$  transition in alkali-metal atoms from  $S_{1/2}$  ground state to  $P_{1/2}$  excited state. The advantage of this transition is that fully polarized atoms become transparent to one sense of circularly polarized

light. Conservation of angular momentum implies that  $S_{1/2}, m_s = 1/2$  state cannot absorb a left circularly polarized photon with  $\hbar$  of angular momentum because there is no  $P_{1/2}, m_s = 3/2$  excited state. Optically dense atomic vapor can then be fully polarized as the light propagates into it and successively polarizes different layers.  $D_1$  transition is also optimal for probing atomic polarization since interaction with circularly polarized light goes from 0 to 100% depending on the orientation of the spins relative to the probe light angular momentum.  $D_2$  line from  $S_{1/2}$  ground state to  $P_{3/2}$  excited state can also be used, particularly for probing, but with a slightly smaller overall efficiency [13].

### 1.3 Sensitivity of Atomic Magnetometers

The fundamental sensitivity of atomic magnetometers is usually dominated by two sources of quantum noise, photon shot noise and spin projection noise. Photon shot noise is due to the discrete nature of photons that are used to measure the spin state of the atoms. A typical probe laser with 1 mW of power contains about  $N_{ph} = 4 \times 10^{15}$  photons passing through the sensor per second. When these photons are detected, their numbers will fluctuate according to Poisson statistics, so the fractional uncertainty in any measurement is on the order of  $(\delta N_{ph}/N_{ph}) = 1/\sqrt{N_{ph}} \approx 10^{-8}$  for a 1 second measurement. For example, fractional absorption of light passing through a vapor cell can be measured with such precision.

In many magnetometers, one monitors optical rotation of the polarization plane of linearly polarized light passing through the sensor, instead of light absorption. Linearly polarized light wave can be written as a sum of right and left circularly polarized waves. Rotation of the plane of linear polarization is due to a phase difference that develops between the two circularly polarized wave components. When the probe light's frequency is detuned from the optical resonance, it primarily has dispersive interactions with atoms, resulting in a change of the index of refraction for the light. The index of refraction for circularly polarized light depends on the spin polarization of the atoms because angular momentum selection rules also apply to virtual transitions that govern dispersive light interactions. For example, for fully polarized atoms, one sense of circularly polarized light experiences a phase delay due to a change in the index of refraction, while light with the other sense of circular polarization has no phase delay. The resulting polarization plane rotation can be measured using a balanced polarimeter or other optical polarimetry techniques. The noise in the measurements of the angle  $\delta\theta$  is also proportional to  $1/\sqrt{N_{ph}} \approx 10^{-8}$  for a 1 second measurement. Because the frequency of the probe light is detuned from optical resonance, it is not significantly absorbed, so higher transmitted intensity can be measured. There is also a smaller contribution to atom spin relaxation from probe light scattering.

The second fundamental source of noise in atomic magnetometers is atom shot noise. It is due to a finite number of atoms participating in the measurement. Because of the relaxation processes, the spin states of individual atoms are randomly being

flipped in collisions, so the average spin of the ensemble undergoes a random walk. According to the fluctuation-dissipation theorem, the shape of the power spectral density of quantum spin fluctuations in the average spin expectation value  $\mathbf{S}$  is the same as the power spectral density in response for an external spin excitation. For a system described by Bloch equations (1.1), it is given by a Lorentzian lineshape with width equal to  $1/T_2$ . The root mean square of spin fluctuations for  $N_a$  spin-1/2 atoms can be calculated from the quantum uncertainty relationships,  $S_x^2 = S_y^2 = S_z^2 = 1/(4N_a)$ , which gives the area under the Lorentzian spin noise peak in the power spectral density.

To determine which of the two noise sources limit the sensitivity of atomic magnetometers, we need to compare the spectral noise densities of atom shot noise and photon shot noise. One can show quite generally [14] that the ratio of the peak spin noise spectral density  $S_n$  and the photon shot noise spectral density  $P_n$  is equal to the optical density of the probe optical transition on resonance,  $S_n/P_n = \text{OD}$ . The optical density OD is defined as the product of cell length  $l$ , the density of atoms per unit volume  $n$ , and the probe light resonant absorption cross-section  $\sigma_0$ ,  $\text{OD} = nl\sigma_0$ . For unpolarized light tuned to optical resonance, the fraction of light intensity transmitted through the cell is simply equal to  $\exp(-\text{OD})$ . One can see that for transmission monitoring the optical density on resonance cannot significantly exceed unity; otherwise, most light will be absorbed. For optical rotation measurements, OD on resonance is not limited in the same way because the probe laser is actually detuned far off resonance, where the optical absorption cross-section is much smaller than the cross-section on resonance  $\sigma_0$ .

Ultimately, probe photon shot noise and atom shot noise add in quadrature. For optimal sensitivity, one would like to have  $\text{OD} \gg 1$  so the photon shot noise does not contribute significantly to the total noise. In most cases, it is sufficient that atom shot noise exceeds photon shot noise by only a factor of 2 or so. But having a very large OD can lead to further improvement in sensitivity by utilizing quantum correlations in the atomic vapor resulting in spin-squeezing [15].

In the regime where atom shot noise dominates, one can derive a general limit on the magnetic field sensitivity of atomic magnetometers, known as the Standard Quantum Limit, or SQL. For example in a pulsed magnetometer operating near-zero total magnetic field, one can monitor spin precession for a time on the order of  $T_2$  starting with full spin polarization in the  $\hat{z}$  direction,  $S_z = 1/2$ . In this time, interval  $S_x$  will develop a finite value on the order of  $S_x \approx \gamma B_y T_2/2$  due to precession in  $B_y$  field. A measurement of  $S_x$  will have an uncertainty equal to  $\delta S_x = \sqrt{\langle S_x^2 \rangle} = 1/(2\sqrt{N_a})$  due to atom shot noise. It can be translated into an uncertainty on the magnetic field  $\delta B_y = 1/(\gamma T_2 \sqrt{N_a})$ . This measurement can be repeated and averaged  $t/T_2$  times over a total time  $t$ , giving an uncertainty  $\delta B_y = 1/\gamma \sqrt{N_a T_2 t}$ . The key factor determining sensitivity is the product of number of atoms  $N_a$  and their coherence time  $T_2$ . One can write  $N_a = nV_c$ , where  $n$  is the density of atoms per unit volume and  $V_c$  is the cell volume. The relaxation time, if it is dominated by the collisions between the atoms being measured, can be written as  $1/T_2 = n\bar{v}\sigma_r$ , where  $\bar{v}$  is the average thermal velocity of the atoms and  $\sigma_r$  is their



spin relaxation collisional cross-section. This gives magnetic field sensitivity after a total measurement time  $t$ :

$$\delta B_y = \frac{1}{\gamma} \sqrt{\frac{\bar{v} \sigma_r}{V_c t}}. \quad (1.2)$$

This equation is independent of the density of atoms, as long as their density is sufficiently high that collisions between them dominate spin relaxation, instead of atom collisions with cell walls or a buffer gas. For a given cell volume  $V_c$ , the best sensitivity is then solely determined by the spin relaxation collision cross-section  $\sigma_r$  and collisional velocity  $\bar{v}$ .

## 1.4 Alkali-Metal Atomic Magnetometers

For alkali-metal atoms most commonly used in magnetometers, the spin relaxation cross-section has a non-trivial behavior because of the relatively complex structure of the atomic ground state. Alkali atoms used in atomic magnetometers have nuclear spin  $I = 3/2, 5/2$ , or  $7/2$ , depending on the atom and isotope. Each atom can occupy one of two possible hyperfine states with  $F = I + 1/2$  or  $F = I - 1/2$ . The two hyperfine states have nearly opposite gyromagnetic ratios because the magnetic moment is dominated by the electron spin that is either parallel or anti-parallel to the total spin of the atom. Hence, a collection of alkali-metal atoms actually consists of two separate populations, one precessing clock-wise and another counter-clockwise around the magnetic field.

When two atoms collide, their electron spins have strong interactions, while the nuclear spins remain shielded by the electron cloud and do not actively participate in the collision. The strongest interaction is due to the so-called spin-exchange collisions, which are described by a Hamiltonian  $H_{se} = J_{ex} \mathbf{S}_1 \cdot \mathbf{S}_2$ . The exchange energy  $J_{ex}$  is on the order of the molecular binding energy between the two atoms, about 1 eV or  $10^{14}$  Hz. So during a typical atomic collision at thermal energies that lasts around  $10^{-12}$  sec, the spins undergo many revolutions around each other. However, the total spin of the colliding pair  $\mathbf{S}_t = \mathbf{S}_1 + \mathbf{S}_2$  is conserved because it commutes with  $H_{se}$ . The nuclear spins are not significantly perturbed during the collision because hyperfine interaction is relatively weak on this timescale, on the order of  $10^{10}$  Hz. After the collision, rotated electron spin states result in a change of the hyperfine eigenstates, but the total spin of the two atoms,  $\mathbf{F}_t = \mathbf{F}_1 + \mathbf{F}_2 = \mathbf{S}_t + \mathbf{I}_t$ , is conserved. Hence, spin-exchange collisions do not result in spin relaxation immediately after the collision. The loss of coherence only occurs over the time scale of the Larmor frequency as the atoms in the two hyperfine states precess in the opposite direction around the magnetic field.

Spin-exchange collisions between alkali-metal atoms have a cross-section of about  $\sigma_{se} = 2 \times 10^{-14} \text{cm}^2$ , on the order of the geometrical cross-section of the

atoms. It is often the largest contribution to  $T_2$  relaxation. Plugging this cross-section into Eq. (1.2) for  $\sigma_r$ , we get a fundamental sensitivity on the order of 1 fT/Hz<sup>1/2</sup> for a cell with 1 cm<sup>3</sup> volume. This is comparable to the sensitivity of low-temperature SQUID magnetometers with a 1-cm diameter pick-up coil. But in practice it is difficult for alkali-metal magnetometers to reach this level of sensitivity since we only considered one source of spin relaxation and assumed perfect detection efficiency. Hence, atomic magnetometers limited by spin-exchange collisions cannot compete in sensitivity with state-of-the-art SQUID magnetometers of comparable size.

### ***1.4.1 Spin-Exchange Relaxation-Free Alkali-Metal Magnetometers***

Spin-exchange collisions do not necessarily contribute to  $T_2$  relaxation because they do not immediately destroy the total angular momentum of the colliding atoms. Spin-exchange relaxation can be suppressed in several ways. If the atoms are placed in a very low magnetic field, then their Larmor precession frequency can be much slower than the rate of spin-exchange collisions. In this regime, fast spin-exchange collisions prevent spins in the two hyperfine states from precessing in opposite directions around the magnetic field in a process similar to motional narrowing in NMR [16]. The populations in the two hyperfine states become locked together by fast spin exchange and precess together. This results in a kind of tug-of-war between the two states that normally precess in opposite directions. As a result, the rate of spin precession slows down and becomes a function of spin polarization in the alkali-metal vapor [17]. Normally, this is not a desirable property since atomic magnetometers rely on a constant proportionality between the Larmor frequency and the magnetic field. However, if the magnetometer is operated very close to zero magnetic field, then changes in the gyromagnetic ratio are less important since the zero-frequency point at zero field is still well-defined.

In this spin-exchange relaxation-free (SERF) regime,  $T_2$  is dominated by the so-called spin-destruction collisions. In these collisions, the spin angular momentum of the colliding atoms is transferred to the orbital angular momentum of the colliding pair, which is quickly lost in other collisions. Spin-destruction collisions can include collisions between alkali-metal atoms and collisions with buffer gas or cell walls. If the density of alkali atoms is sufficiently high that collisions between them dominate, then one can obtain a fundamental limit on sensitivity using Eq. (1.2) with  $\sigma_r$  equal to the spin-destruction cross-section. These cross-sections vary from about  $\sigma_r = 10^{-18}\text{cm}^2$  for K atoms to  $\sigma_r = 10^{-16}\text{cm}^2$  for Cs atoms. With the smaller spin relaxation cross-section, one can obtain much better fundamental sensitivity, on the order of 10 aT/Hz<sup>1/2</sup> for a 1 cm<sup>3</sup> cell in K [18]. In this regime, the practical sensitivity of spin-exchange relaxation-free magnetometers can indeed exceed the sensitivity of SQUID magnetometers with comparable size pick-up coils [19, 20].

Operating near-zero field is not the only method of suppressing spin-exchange relaxation. Another approach is to create very high spin polarization in the alkali-metal vapor, so most atoms are fully polarized in the  $F = S + I$  hyperfine state. When two fully polarized atoms collide, they cannot be transferred to another state while preserving the total spin polarization, so the effect of collisions is suppressed. This approach requires maintaining high degree of spin polarization in the alkali vapor. However, the optical pumping rate  $R$  in Eq. (1.1) also contributes to loss of spin coherence. One approach involves careful balancing of optical pumping rate with spin relaxation rate [21]. Another approach is to use pulsed optical pumping, where spin-exchange relaxation is temporarily suppressed immediately after application of a strong optical pumping pulse [22]. These methods do not completely eliminate the effects of spin-exchange relaxation but can reduce its effects.

## 1.5 Practical Challenges in Operation of Atomic Magnetometers

So far we have reviewed fundamental aspects of atomic magnetometer operation. However, to make a practical sensor, one needs to take into account many additional constraints. In the following, I will summarize some of these challenges in general terms; there are many different approaches for addressing them that will be discussed in later chapters.

First, one typically needs to include a modulation mechanism in the operating scheme because measurements limited by quantum noise are very challenging in the frequency range of 1 Hz–1 kHz that is typical for biomagnetic signals. By modulating the signal in some way, one can move the detection frequency to higher values, typically 1 kHz or above, and use a form of lock-in detection. Optical rotation or absorption measurements on the atomic vapor can be performed by modulating the polarization or wavelength of the probe laser beam. The advantage of probe beam modulation method is that it does not perturb the atoms, allowing one to obtain the highest sensitivity. However, it cannot always separate optical effects of the atoms from background optical signals caused by changes in birefringence, optical interference, or transmission of the cell. Another approach is to apply a magnetic field modulation in order to induce rotation of the atomic spins, which then provide a modulation of the optical signal. Modulation of the optical signal by applying an external  $B(t)$  field to the spins effectively eliminates optical background effects but typically somewhat reduces the sensitivity since the spins are perturbed away from optimal configuration for highest sensitivity. It also places stringent requirements on the low-noise properties of the modulating field that is added on top of the fields being measured. In a scalar atomic magnetometer, the spins already precess around the magnetic field at a Larmor frequency much greater than 1 kHz. In this case, one does not need to apply additional modulation, but the source of the bias field needs to be very stable to achieve good sensitivity in an individual magnetometer.

In most cases, biomagnetic signals are detected using a magnetic gradiometer, which compares signals from two or more nearby magnetometers. This allows one to separate local sources of the biomagnetic field, which vary sharply with distance from the source, from distant sources of magnetic interference that are more uniform on the scale of a few centimeters. For atomic gradiometers, it is usually easiest to subtract signals from two or more separate magnetometers. There is no simple analogue to a gradiometer pick-up coil for SQUID sensors since each atom interacts individually with the total magnetic field. The performance of a magnetic gradiometer can be characterized in terms of a common-mode rejection ratio (CMRR) to indicate how well it cancels a uniform magnetic field. For a vector magnetometer, it is important that the axes of the two sensors are well aligned so they measure the same field components. It is also important that the calibration constants are stable for both magnetometers and they have similar bandwidths, so their response to a uniform field cancels for all times and at all frequencies. Each of these requirements represents some challenge to vector atomic magnetometers since their vector axes, sensitivity, and bandwidth depend on many details of operation. For scalar atomic magnetometers, the requirements are somewhat relaxed since a common vector axis is defined by the total magnetic field and the sensitivity is determined by the gyromagnetic ratio that is expressed in terms of fundamental constants. When many magnetometers are operated in an array, it is possible to use post-processing analysis techniques, such as independent component analysis, to separate distant sources of signal that are common to many channels from more localized sources. Post-processing techniques or frequent calibration can also correct for inaccuracies in the alignment, calibration, and bandwidth between multiple sensors.

In many biomagnetic studies, one of the goals is to localize the sources of the magnetic field signals based on information from multiple sensors. As a prerequisite for such localization, one has to first localize the position of each sensor. This represents some challenge for atomic sensors since the magnetic field measurement volume is defined not in terms of a physical structure, but in terms of optically active atoms. For example, if only some part of the vapor cell is polarized, then only those atoms contribute to the signal. In cells that rely on anti-relaxation wall coatings to limit atomic spin relaxation and do not contain any buffer gas, the atoms diffuse very quickly across the cell, so they sample fairly uniformly the whole cell volume. In cells that rely on buffer gas to limit spin relaxation on cell walls, the buffer gas pressure is typically adjusted so the diffusion time from the center to the edge of the cell is comparable to the spin coherence time due to other sources of relaxation. As a result, the distribution of polarized spins can even evolve during a single measurement. To eliminate these uncertainties, the effective positions of the sensors are usually localized during the experiment by applying a calibrated magnetic field gradient and measuring the resulting signals in the magnetometer array.

Slow diffusion of atoms in the cell can also be used to create multiple magnetic sensors in a single cell. For example, if the probe laser beam is imaged on a multi-channel photodiode, then each photodiode segment will record a signal proportional

to the magnetic field averaged along a line of polarized atoms illuminated by that segment of the probe laser beam. In this way, many-channel systems can be created using many common components. The advantage of this approach is relative simplicity in making detailed maps of the magnetic field and localization of biomagnetic sources [23]. However, the geometry of the field measurement locations is more restricted by the optical constraints. Planar images can be more easily measured, which is sufficient for magnetocardiography. However, for magnetoencephalography, it is desirable to place sensors on the surface of a sphere, which is harder to realize using common beam approaches. For this application, many small atomic sensors with integrated lasers and optics can be flexibly placed around the subject's head.

As with many other sensors, one usually has a choice in operating a magnetometer in a closed-loop feedback mode or in open loop. Open-loop sensors provide a signal proportional to the magnetic field being measured. Vector atomic magnetometers usually have a relatively narrow dynamic range, on the order of 10–100 nT, which is related to the spin relaxation time by the gyromagnetic ratio,  $\Delta B \sim \gamma / T_2$ . The total field has to be maintained well below this level to obtain a linear sensor response. In closed-loop operation, the magnetic field near the sensor is maintained close to zero using feedback coils. The electric currents flowing in these coils then provide a measure of the magnetic field. An advantage of this approach is that the linear dynamic range of the sensor can be extended and in some cases the bandwidth of the response can be improved as well. When operating arrays of sensors, the feedback coils can create cross-talk and generate local magnetic field gradients for other sensors. For vector sensors, it is important to zero out all 3 magnetic field components. Therefore, it is advantageous to have a sensor that can simultaneously measure 2 or more field components [24]. Scalar atomic magnetometers can be operated in feedback mode or in free induction decay (FID) mode. In feedback mode, one usually adjusts the frequency of spin excitation to match the Larmor frequency. In FID mode, one simply measures the Larmor precession frequency of the atoms. Since the measured quantity in this case is a frequency, it can be measured with much higher fractional precision than an analog voltage or current signal. Therefore, scalar magnetometers can maintain a much larger dynamic range without losing sensitivity or linearity.

Biomagnetic measurements are usually performed within magnetic shields to screen out external noise sources as well as the Earth's magnetic field. Atomic magnetometers can operate within typical shielded rooms used for biomagnetic studies. However, they typically need better control of the magnetic fields inside the shields because atoms are sensitive to the total value of the field, not just a change in the field typical for SQUID sensors. Usually, the total field inside the shield should be zeroed out, either globally with large coils or locally with small coils near each sensor. However, local field compensation can also increase magnetic field gradients. Magnetic shielding systems for atomic magnetometers can be smaller than those for SQUID systems since they do not require an integrated cryogenic dewar. Scalar atomic magnetometers are particularly well suited for operation

outside of the magnetic shields since they can distinguish a small biomagnetic signal on top of a large Earth's field [25].

Biomagnetic measurements require placement of the sensors as close as possible to living organisms near room temperature. This represents a particular challenge for thermal insulation of SQUID magnetometers since they operate at liquid helium or liquid nitrogen temperatures. Atomic magnetometers typically operate at or above room temperature. In particular, Cs has fairly high vapor pressure so strong signals can be obtained already at 35°C. For other atoms, such as Rb or K, one has to heat the cell to 100–150°C to achieve sufficient alkali-metal density. These cells have to be thermally insulated. Since heating power is not as limited as cooling power for superconducting sensors, the main limitation is the need to maintain reasonable temperature less than about 40°C on side of the sensor in contact with the subject. Magnetometers using optical pumping of metastable  $^4\text{He}$  atoms or using NV centers in diamond can operate at virtually any temperature since the density of atoms is not controlled by saturated vapor pressure.

## 1.6 Conclusions

Optically pumped magnetometers provide a new, rapidly developing method for detection of biomagnetic fields. They can be operated in several different modes with widely varying properties. Their intrinsic simplicity holds promise for widespread use in biomagnetic applications. With proper optimization, they can achieve quantum-limited sensitivity and exceed the performance of commonly used SQUID sensors. Several atomic magnetometer systems have already been developed and used for a variety of biomagnetic field recordings. The present challenge is in the development of an economical approach that combines most positive features of the atomic sensors into a robust device. Perhaps, several approaches will ultimately find use depending on particular application.

## References

1. Bell, W. E., & Bloom, A. L. (1957). *Physical Review*, 107, 1559. <https://link.aps.org/doi/10.1103/PhysRev.107.1559>.
2. Brossel, J., & Bitter, F. (1952). *Physical Review*, 86, 308. <https://link.aps.org/doi/10.1103/PhysRev.86.308>.
3. Hawkins, W. B., & Dicke, R. H. (1953). *Physical Review*, 91, 1008. <https://link.aps.org/doi/10.1103/PhysRev.91.1008>.
4. Bloom, A. L. (1962). *Applied Optics*, 1(1), 61. <https://opg.optica.org/ao/abstract.cfm?URI=ao-1-1-61>.
5. Dupont-Roc, J., Haroche, S., & Cohen-Tannoudji, C. (1969). *Physics Letters A*, 28(9), 638. <https://www.sciencedirect.com/science/article/pii/0375960169904800>.
6. Livanov, M. N., Kozlov, A. N., Korinevskii, A. V., Markin, V. P., Sinel'nikova, S. E., & Holodov, Y. A. (1978). *Doklady Akademii Nauk SSSR*, 238(1), 253.

7. Livanov, M. N., Kozlov, A. N., Sinelnikova, S. E., Kholodov, J. A., Markin, V. P., Gorbach, A. M., & Korinewsky, A. V. (1981). *Advances in Cardiology*, 28, 78. <https://doi.org/10.1159/000391945>.
8. Bison, G., Wynands, R., & Weis, A. (2003). *Physics Letters B*, 76(3), 325. <https://doi.org/10.1007/s00340-003-1120-z>.
9. Xia, H., Ben-Amar Baranga, A., Hoffman, D., & Romalis, M. V. (2006). *Applied Physics Letters*, 89(21), 211104. <https://doi.org/10.1063/1.2392722>.
10. Bouchiat, M. A., & Brossel, J. (1966). *Physical Review*, 147, 41. <https://link.aps.org/doi/10.1103/PhysRev.147.41>.
11. Bell, W. E., & Bloom, A. L. (1961). *Physical Review Letters*, 6, 280. <https://link.aps.org/doi/10.1103/PhysRevLett.6.280>.
12. Budker, D., Kimball, D. F., Rochester, S. M., Yashchuk, V. V., & Zolotarev, M. (2000). *Physical Review A*, 62, 043403. <https://link.aps.org/doi/10.1103/PhysRevA.62.043403>.
13. Johnson, C., Schwindt, P. D. D., & Weisend, M. (2010). *Applied Physics Letters*, 97(24), 243703. <https://doi.org/10.1063/1.3522648>.
14. Romalis, M. V. (2013). *Optical Magnetometry*. In D. Budker, D.F. Jackson Kimball, (Eds.) Cambridge University Press, pp. 25–39. <https://doi.org/10.1017/CBO9780511846380.003>.
15. Bouchoule, I., & Mølmer, K. (2002). *Physical Review A*, 66, 043811. <https://link.aps.org/doi/10.1103/PhysRevA.66.043811>.
16. Happer, W., & Tang, H. (1973). *Physical Review Letters*, 31, 273. <https://link.aps.org/doi/10.1103/PhysRevLett.31.273>.
17. Savukov, I. M., & Romalis, M. V. (2005). *Physical Review A*, 71, 023405. <https://link.aps.org/doi/10.1103/PhysRevA.71.023405>.
18. Kominis, I. K., Kornack, T. W., Allred, J. C., & Romalis, M. V. (2003). *Nature*, 422(6932), 596. <https://doi.org/10.1038/nature01484>.
19. Dang, H. B., Maloof, A. C., & Romalis, M. V. (2010). *Applied Physics Letters*, 97(15), 151110. <https://doi.org/10.1063/1.3491215>.
20. Storm, J. H., Hömmen, P., Drung, D., & Körber, R. (2017). *Applied Physics Letters*, 110(7), 072603. <https://doi.org/10.1063/1.4976823>.
21. Smullin, S. J., Savukov, I. M., Vasilakis, G., Ghosh, R. K., & Romalis, M. V. (2009). *Physical Review A*, 80, 033420. <https://link.aps.org/doi/10.1103/PhysRevA.80.033420>.
22. Sheng, D., Li, S., Dural, N., & Romalis, M. V. (2013). *Physical Review Letters*, 110, 160802. <https://link.aps.org/doi/10.1103/PhysRevLett.110.160802>.
23. Kim, K., Begus, S., Xia, H., Lee, S. K., Jazbinsek, V., Trontelj, Z., & Romalis, M. V. (2014). *NeuroImage*, 89, 143. <https://www.sciencedirect.com/science/article/pii/S105381191301063X>.
24. Li, Z., Wakai, R. T., & Walker, T. G. (2006). *Applied Physics Letters*, 89(13), 134105. <https://doi.org/10.1063/1.2357553>.
25. Limes, M., Foley, E., Kornack, T., Caliga, S., McBride, S., Braun, A., Lee, W., Lucivero, V., & Romalis, M. (2020). *Physical Review Applied*, 14, 011002. <https://link.aps.org/doi/10.1103/PhysRevApplied.14.011002>.

# Chapter 2

## Optically Pumped Magnetometers Compatible with Large Transient Magnetic Fields



Nicholas Nardelli, Sean Krzyzewski, and Svenja Knappe

**Abstract** Optically pumped magnetometers have seen an increased interest in applications such as magnetoencephalography where extremely small magnetic fields produced in the brain must be distinguished from the large and noisy magnetic background of the world. In environments where magnetic shielding may be weak, optically pumped gradiometers are useful for separating out signals of interest from magnetic interference. We describe magnetic sensors operating in closed-loop mode, whereby a feedback signal is used to continuously keep the atoms in a zero-field environment. This allows for a larger linear operating range of the sensor, reduces the need for frequent re-calibration, increases the common-mode rejection ratio of the gradiometers, and increases the linearity as compared to open-loop measurements. We also discuss a specific application of atomic magnetometers in a weakly shielded environment where large magnetic field pulses are used to stimulate a subject's brain. Atomic magnetometers are uniquely suited to quickly recover and take low-noise measurements to probe the resulting neuronal currents after stimulation events.

**Keywords** Optically pumped magnetometer · Magnetoencephalography · Superconducting quantum interference device · Quantum sensor · Multichannel · Electron spin resonance · Spin-exchange relaxation-free · Alkali-metal vapor cell · Atomic magnetometer · Optical magnetometer

---

N. Nardelli (✉) · S. Krzyzewski  
University of Colorado Boulder, Boulder, CO, USA

S. Knappe  
University of Colorado Boulder, Boulder, CO, USA

FieldLine Inc., Boulder, CO, USA  
e-mail: [svenja.knappe@colorado.edu](mailto:svenja.knappe@colorado.edu)



## 2.1 Introduction

Magnetoencephalography (MEG) is a technique for measuring weak magnetic signals which originate in the brain due to small neuronal currents [1]. It is a powerful tool for noninvasive diagnostic brain imaging as well as research into cortical activity at millisecond timescales. However, the current MEG technology based on superconducting quantum interference devices (SQUIDs) is expensive, requires a magnetically shielded room with several layers of ferromagnetic shielding material, as well as a liquid helium system [2, 3]. As such, hospitals have been slow to embrace MEG technology [4].

Optically pumped magnetometers (OPMs) [5] have emerged as an exciting new alternative to SQUIDs for bio-magnetic sensing, especially MEG [6–8]. Because they do not need cryogenic cooling, OPMs can be placed within millimeters of the scalp and can be manipulated independently to conform to heads of different sizes.

OPMs operating in the spin-exchange relaxation-free (SERF) regime [9, 10] typically require background fields in the nanotesla range to ensure that the spin-exchange collision rate is much faster than the Larmor precession frequency. In addition, magnetometer calibration factors, linewidths, and sensitive directions are dependent on changes in background field. Therefore, OPM-based MEG requires a high level of magnetic shielding that may not be satisfied by rooms constructed for SQUID-based MEG, which typically have residual fields of tens of nanotesla, as well as large magnetic gradients (tens of nT/m).

To mitigate the background and gradient field, nulling coils are added to the sensor heads that control the local magnetic field environment for each sensor. In addition, several groups have added large global offset coils inside the passively shielded rooms, which actively null offset and gradient magnetic fields in the vicinity of a subject's head [11–14]. Nulling the background field and reducing the gradient relax the restriction that a subject's head must remain immobile. Since OPMs are small enough to be mounted on a helmet, this opens the possibility of studying subjects under new paradigms or studying subjects who cannot remain still for an extended amount of time, such as small children or patients with Parkinson's Disease.

In several applications, the static background fields can remain small, but large transient magnetic fields are present. In low-field nuclear magnetic resonance (NMR), for example, often a large prepolarization field is applied. Once the field is switched off, atomic magnetometers can be used to measure the small relaxing magnetization of the sample [15]. For some magnetic nanoparticle detection schemes, a large field is used to orient the nanoparticle ensemble, and the relaxation of the nanoparticles can be detected or imaged [16–18]. In transcranial magnetic stimulation (TMS), large magnetic field pulses are used to polarize or de-polarize neurons in the brain for therapy purposes [19–22]. OPMs are good candidates to measure small magnetizations immediately after large field pulses, as the dead time depends theoretically only on the time it takes to re-polarize the spin ensemble,

which is typically on the order of a few milliseconds, but could be as low as microseconds, if enough pump-laser power is available.

### 2.1.1 Brief Introduction to SERF OPMs

Although there are many types of atomic magnetometers, we focus on miniaturized optically pumped magnetometers operating in the spin-exchange relaxation-free regime [9, 10]. In this regime, spin decoherence due to spin-exchange collisions is suppressed, which allows a large number of alkali atoms to coherently contribute to a magnetic signal despite occupying a small volume [23]. This is achieved by first, producing a large spin polarization through optical pumping with circularly polarized light and second, by increasing the rate of collisions through heating the atomic vapor, while also reducing the Larmor precession rate by shielding the atoms from large external fields. This is illustrated in Fig. 2.1.

To build a compact SERF magnetometer, a microfabricated vapor cell ( $3 \times 3 \times 2 \text{ mm}^3$ , displayed in Fig. 2.2) is filled with a droplet of  $^{87}\text{Rb}$  and approximately 1 amg  $\text{N}_2$  gas. The  $\text{N}_2$  gas serves as both a quenching gas to prevent radiation trapping and as a buffer gas to prevent the diffusion of  $^{87}\text{Rb}$  atoms to the cell walls, both of which cause atomic spin decoherence and linewidth broadening [24–27].

In the OPMs described here, the vapor cells are optically heated to approximately  $150^\circ\text{C}$  through the absorption of light from a heating laser at  $1540 \text{ nm}$  by colored glass filters attached to the windows of the vapor cells [28, 29]. The cells are suspended on a web of polyimide and vacuum packaged inside a small enclosure made from silicon and glass [30]. This reduces the temperature at the tip of the sensor that touches the patient, while maintaining a minimal distance of  $4.5 \text{ mm}$  between the center of the cell and the outside housing of the OPM sensor.

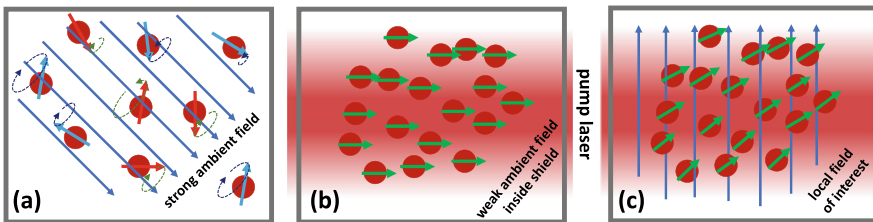


**Fig. 2.1** (a) In a large magnetic field (e.g., Earth’s field) at room temperature, the rate of Larmor precession is faster than the rate of collisions, yielding very low spin coherence. (b) Circularly polarized light aligns spins along laser propagation direction. (c) In a small nonzero-field ( $<5 \text{ nT}$ ) at high temperature ( $150^\circ\text{C}$ ), the balance between optical pumping and coherent precession causes a static polarization, which is not aligned with the optical pumping direction

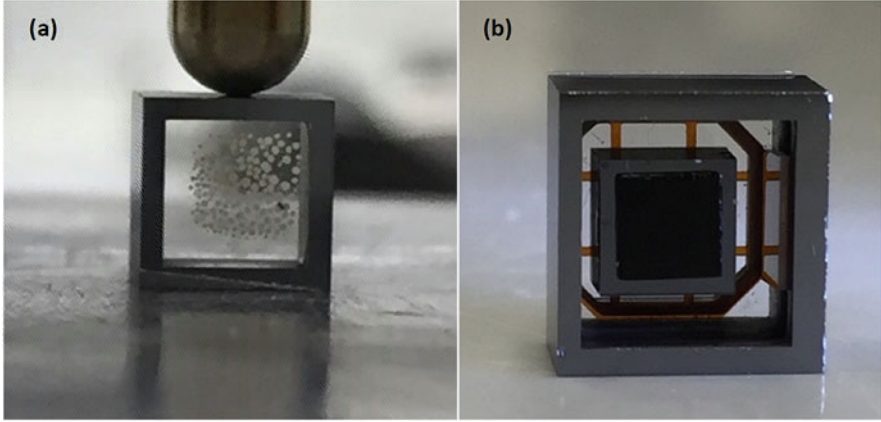


**Fig. 2.2** (a) Photograph of a microfabricated  $^{87}\text{Rb}$  vapor cell ( $3 \times 3 \times 2 \text{ mm}^3$ ). (b) Photograph of a cell suspended on a Kapton webbing inside a vacuum package. A colored glass filter on the front of the cell is used to absorb 1540 nm light to optically heat the vapor cell

Circularly polarized light at 795 nm, resonant with the D1 transition, is used to optically pump the atoms. The transmitted light passed through the cell, is detected and the power is used to infer the magnetic field [31, 32].

## 2.2 Methods for Stable Operation in a Noisy Environment

### 2.2.1 Closed-Loop Mode

Most MEG systems based on OPMs to date are operated in “open-loop” mode. In the single-beam approach described above, the resonance line has the shape of an absorptive Lorentzian with a width of around 20 nT, when the transverse magnetic field is scanned around zero (Fig. 2.3a). A small oscillating magnetic field is applied perpendicular to the laser axis to define the sensitive axis of the directional magnetometer. When demodulating the photodiode signal at the frequency of the field modulation with a phase-sensitive detector, the line shape is the derivative of the original signal (Fig. 2.3b). The magnetometer is sensitive in first order to fields in the direction of the field modulation. Around zero magnetic field, the output signal is approximately linear with magnetic field. The slope of this resonance is typically calibrated before every MEG recording, since it depends on many parameters: residual magnetic fields and gradients in all directions, the cell temperature, pump intensity, and modulation parameters.

During a measurement, magnetic resonance linewidths must remain stable or calibration values (i.e., resonance slopes) will change and render results unreliable.

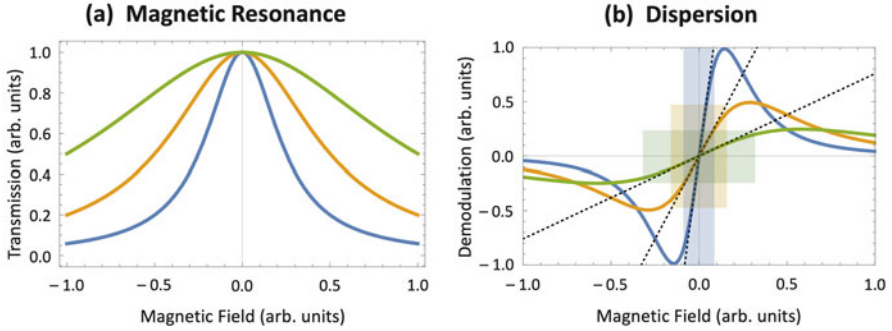


**Fig. 2.3** (a) Magnetic resonance for three atomic samples with varying linewidths and (b) the corresponding demodulated profiles after passing the signal through a phase-sensitive detector. The dotted black lines show the linear approximation at zero magnetic field and the colored boxes show the span over which each dispersion is at least 95% linear

In poorly shielded environments, background fields can change at a level that substantially alters open-loop field calibrations over the time of minutes.

In addition, the slope can only be approximated as linear over a limited range of field values away from zero, referred to as the linear range. Typically, there is a trade-off between linear range and sensitivity since a more-sensitive OPM (steeper slope) has a much smaller linear range than a less-sensitive OPM (flatter slope), which remains linear over a much broader range of magnetic field values. This is shown by the three curves in Fig. 2.3b where colored boxes indicate the linear range of each dispersion.

Finally, in the presence of large transverse background fields, the OPM becomes sensitive to transverse field directions and the effective orientation of the magnetic field reading tilts [33, 34]. These effects limit the localization accuracy and effectiveness of noise rejection methods.

Closed-loop operation offers a solution to reduce the drifting calibration factor and extend the linear operating range. This has been implemented for a single magnetometer axis in a number of magnetometers [35, 36] and MEG arrays [37, 38]. In this scheme, the current coils used to supply the field modulation for the phase-sensitive detection are used to also apply a nulling field over the bandwidth of the magnetometer through a control feedback loop (such as a PID). The current required to create the nulling field serves as the measurement that represents magnetic field readings.

The control loop allows for changes in the slope of the dispersion while still being able to maintain zero-field, and because of this, the only calibration involves the current-to-field conversion of the current coils themselves. Since the coil geometry is fixed, so is the calibration factor. In this way, closed-loop OPMs can be subject to instabilities of any of the parameters that affect the atomic linewidth or amplitude while maintaining a more stable magnetic field reading. It should be noted that, although magnetic signals are recorded reliably as linewidth increases, sensor

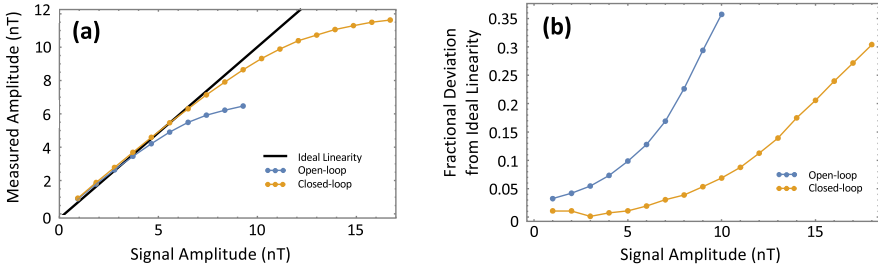


**Fig. 2.4** Linearity of magnetometer response. **(a)** Magnetometer response in open-loop (blue) and closed-loop (yellow) mode as field modulation amplitude increases. **(b)** Fractional deviation of open-/closed-loop magnetometers in **(a)** from the ideal linearity (black line). (Reprinted from Ref. [38] with the permission of Springer)

baseline noise increases with linewidth, yielding a worse SNR and sensitivity than an OPM operating under ideal conditions. Additional modulation coils with different modulation frequencies or phases can be added to null the field in the other two directions to prevent the resonance from broadening due to transverse background fields. This tri-axial closed-loop scheme has been implemented recently in Helium-4 magnetometer arrays [39, 40].

In theory, a closed-loop OPM is linear over a large operating range because the feedback keeps the alkali atoms at the center of the dispersion line. As such, OPMs can measure field variations on top of large rapidly drifting background fields. In practice, the operating range is typically limited by several factors, including the electronics driving the current through the feedback coils and the gain and dynamic range of the feedback loop. The increase in response linearity is demonstrated in Fig. 2.4, where both open-loop and closed-loop operations of the same OPMs are compared.

For MEG measurements, closed-loop OPMs are extremely versatile because they require fewer calibrations. Well-calibrated readings in the presence of background interference are crucial for the large-scale adoption of this technology for MEG.

It can also be useful in developing efficient MEG co-registration schemes with OPMs, which aim to relate the MEG images to the anatomical reference frame deduced from MRI images. Traditionally, head position indicator (HPI) coils are used to localize MEG magnetometers in relation to the head although optical methods are also being developed [41]. Due to the limited linear operating range of OPMs, the signal from the HPI coils can drive nearby OPMs beyond their linear range. A large HPI coil field is needed to ensure that OPMs that are further away can still detect the signal. Closed-loop operation extends the linear range and therefore extends the spatial region of sufficient linearity and co-registration.

When operating a dense MEG array in closed-loop mode, sensor cross-talk becomes a more prominent issue, especially as the spacing between sensors becomes very small. To address this complication for future arrays, a new modulation coil design has been developed with an outer winding that serves to cancel

excess field outside of the coil [42]. This suppresses cross-talk between nearby sensors by more than an order-of-magnitude.

### 2.2.2 *Magnetic Gradiometry*

Magnetic signals originating in the brain are extremely weak (femtotesla to picotesla at the scalp) and are difficult to separate from the increasingly large magnetic background of the modern world. Even inside of the best magnetic shields, low-frequency fields from machines, electronics, and large moving metal objects penetrate at levels large enough to raise the noise floor above many signals of interest. Even vibrations from the floor and walls can couple into sensors and increase noise floors if the OPMs are not properly isolated.

Magnetic gradiometers address some of these issues by adding an additional co-linear OPM as a reference. Figure 2.5 shows an example of a magnetic radial gradiometer used in a recent MEG array [38]. One OPM acts as the “sensing” cell and is located closer to a magnetic source of interest (i.e., on the scalp) and the other acts as the “reference” cell, sampling the noise background in the vicinity and direction of the sensing cell. Brain signals, which very quickly decay with distance, will predominantly be present in the sensing cell located on the scalp, and much reduced in the reference cell located 2 cm away from the sensing cell. Subtraction of these two OPM signals yields a gradiometer which has superior noise properties to either of the constituent OPMs. Hardware gradiometers are routinely implemented in SQUID-based MEG systems [43].

One of the main attractions of magnetic gradiometers is the subtraction of large background fields that are common to both OPMs and may vary in time, making them difficult to disentangle from signals originating in the brain. In weak shields, such as in single-layer magnetically shielded rooms or in cylindrical shields with one open end for human access, magnetic gradiometers are convenient in suppressing background interference, especially for arrays with a small number of OPMs.

The coupling of laser amplitude noise to magnetic noise is also a significant contributor to OPM baseline noise levels. In transmission-based magnetometer schemes utilizing a single photodiode, changes in magnetic field cannot be distinguished from changes in laser intensity and so a high-RIN laser can severely degrade the performance of a magnetometer [44]. In one case, where pump/probe light was delivered to OPMs via a polarization-maintaining fiber over approximately 6 m, floor vibrations coupled into the magnetometer noise via changes to the light polarization in the fiber. These were converted to intensity noise by a polarizer located before the alkali vapor cells. Gradiometers can suppress this common noise, because light is split equally and delivered to both reference and sensing OPM [36].

The magnetic sensitivity for a single gradiometer is shown in Fig. 2.6a, which includes both magnetometer signals and the subtracted gradiometer signal. The quadrature lock-in signal is also shown, which is not sensitive to magnetic field and